MODELING AND ACTIVE CONTROL OF THERMOACOUSTIC INSTABILITIES

André S.P. Niederberger [*] **Bruno B.H. Schuermans** [**]
Lino Guzzella [*]

[*] *Measurement and Control Laboratory, Swiss Federal Institute of Technology, CH-8092 Zurich, Switzerland*
email: niederberger@imrt.mavt.ethz.ch
[**] *ALSTOM Switzerland Ltd.*

Abstract: Due to stringent emission regulations, modern gas turbines work in lean premixed mode and thermoacoustic instabilities are often observed. They cause mechanical damage and therefore have to be reduced. This paper describes the development of an acoustic network model for a lab-scale lean premixed methane combustor at ETH Zurich. The model is verified against experimental data and is then used to develop an H_∞-controller, with special concern given to fundamental limits imposed by the system. The proposed controller is then verified in simulations.

Keywords: Gas Turbines, Control Oriented Models, Active Control, Robust Control, Power Systems

1. INTRODUCTION

Modern gas turbines have to comply with continually more stringent emission regulations (NO_x, CO etc.), which led to the development of lean premixed combustion systems. They operate with excess air to lower the combustion temperature to decrease NO_x levels described by the Zeldovich mechanism. However, this makes the combustor prone to thermoacoustic instabilities and causes mechanical damage, higher heat transfer to walls, noise and pollutant emissions. This phenomenon is observed not only in gas turbines, but also in rocket motors, ramjets, afterburners, and domestic burners. Thermoacoustic instabilities arise due to a feedback loop involving fluctuations in pressure, velocity and heat release. Lord Rayleigh (Rayleigh, 1878) first noted that if the heat release is in phase with the pressure fluctuations, the instability grows, while combustion is stable if they are out of phase. Note that this criterion is defined over space, so that at certain points in the combustor damping may prevail, while at others the instability is growing.

1.1 *Mechanisms of Thermoacoustic Instabilities*

Unsteady combustion introduces pressure waves in the combustor which are reflected back from the boundaries and modify combustion, generating a feedback cycle. In a study of a swirl stabilized premix burner (Paschereit *et al.*, 1999), it was found that large coherent structures are associated with instability. The interaction between flow instabilities and acoustic resonant modes excites unstable modes, leading to periodic combustion in large-scale structures. Specifically, the recirculation wakelike zone near the combustor axis and the shear layer instabilities at the dump plane are identified as being coupled to unstable modes. Fuel feedline dynamics are another mechanism causing equivalence ratio fluctuations (Annaswamy and Ghoniem, 2002).

1.2 *Models of Thermoacoustic Instabilities*

In general, models can be obtained from purely experimental data, or based on physical principles (Dowling and Stow, 2003), or from a combination of the two. Another way of developing models is to identify them with an appropriate structure, for instance an ARX structure. An approach where uncertain parameters in a physical model are determined using measurements is presented in (Campos-Delgado *et al.*, 2003*b*).

1.3 *Control of Thermoacoustic Instabilities*

The first passive approaches to the problem consisted of installing baffles and acoustic dampers to increase damping, and changing the flame anchoring, burning mechanism and fuel line piping to break the feedback loop. As new sensor, actuator and computing technology evolved, active control began to be introduced. Available sensors are piezoelectric and moving coil microphones to detect pressure fluctuations, and photodiodes and OH/CH chemiluminescence sensors to measure heat release rates. Actuators introduce perturbations in acoustic pressure, velocity, vorticity, fuel or air mass flow. However, loudspeakers have a very limited control authority. Only the control of the fuel flow, for instance by using secondary fuel injectors, has the potential to successfully counteract the combustion instabilities.
The control algorithms used range from simple phase-shift controllers (Paschereit *et al.*, 1999), to robust LQG/LTR (Campos-Delgado *et al.*, 2003*a*) and H_∞-controllers (Campos-Delgado *et al.*, 2003*b*). Phase-shift control is the simplest strategy, but often generates secondary peaks because of inappropriate phase at frequencies other than the unstable frequency.

2. THE EXPERIMENTAL SETUP

A schematic illustration of the test rig built at ETH Zurich is shown on the left-hand side of Figure 1. Preheated air premixed with methane flows through flow straighteners into a plenum chamber duct. The ALSTOM EV swirl burner stabilizes the flame in recirculation regions near the burner outlet plane, while the combustion gases are guided through a downstream duct and are subsequently discharged. For excitation purposes, loudspeakers are mounted in both ducts upstream and downstream of the burner. The pressure signal is detected by water-cooled microphones distributed along the ducts.

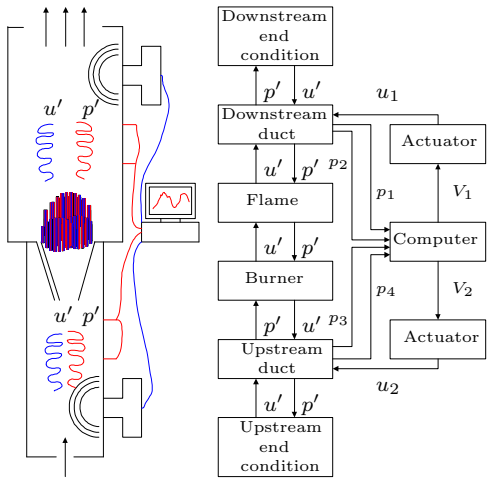

Fig. 1. An illustration of the ETH combustor and of the network model

3. THE ACOUSTIC NETWORK MODEL

Following (Campos-Delgado *et al.*, 2003*b*), the combustor is split into a network of different elements. More specifically, referring to the right-hand side of Figure 1, the model consists of an upstream end condition, where the air enters the upstream plenum chamber, followed by the burner and the flame. The hot gases leave the combustion chamber duct through a downstream end condition. An actuator introduces velocity fluctuations into the system. Pressure and velocity signals are travelling between the individual blocks, whose behavior is represented in matrix form by transfer functions. They are found analytically and relevant parameters are identified experimentally. By judiciously forcing the combustor with the loudspeakers and measuring the pressure at different axial positions, the transfer functions of the different blocks can be determined. More precisely, a dynamic signal analyzer sends a swept sine signal to the loudspeaker and monitors the pressure output of the microphones. The acoustic field is treated as purely longitudinal (the frequencies of interest lie beneath the cutoff frequency $\omega = 1.841c/a$, c being the speed of sound and a the radius of the circular duct). Moreover, the geometrical extent of the burner and the flame are small compared to the wavelengths of the acoustics involved, which allows to take only plane waves into account. In this case, the pressure and velocity fluctuations $p'(t)$ and $u'(t)$, are described by the Riemann invariants $f(t)$ and $g(t)$ (ρ is the density)

$$p'(t) = \rho c(f(t) + g(t)) \tag{1}$$
$$u'(t) = f(t) - g(t) \tag{2}$$

This allows to determine the acoustic velocity at an arbitrary position using only two pressure mea-

surements, because the Riemann invariants have the interesting property that at given positions x_i and x_j with mean flow $\bar{u}$ the following relationship applies: $f(x_j) = f(x_i)e^{-s\frac{x_j - x_i}{c+\bar{u}}}$. It becomes clear from Equation 1 that a *scaled* pressure fluctuation $p'_{sc}(t) = \frac{p'(t)}{\rho c}$ is the signal travelling to and fro in the network model. Once the velocity and pressure evolution on both sides of a network element are known, it is easy to extract the transfer function. In order to determine the transfer matrix of the burner $T^b(s)$, the combustor without flame is excited first with the loudspeakers upstream and then downstream. The transfer function of the flame by itself $T^f(s)$ cannot be measured, but the combined transfer function of the burner and the flame $T^{bf}(s)$ is determined as before with the flame burning. Knowing the burner transfer matrix $T^b(s)$, the flame block can easily be extracted: $T^f(s) = T^{bf}(s){T^b}^{-1}(s)$.
This identification procedure was applied to the combustor burning premixed methane with a preheat temperature of 700K, a mass flow of 36g/s and $\lambda = 2.1$.

3.1 *The Ducts*

Only plane longitudinal waves can exist in the frequency range considered. A modal expansion method of the acoustic equation is presented in (Schuermans *et al.*, 2003), where a velocity input occurs at x_j and the pressure is read out at x_k, yielding the following state-space representation for one mode n:

$$\dot{x}(t) = A_n x(t) + B_{nj} u'(t) \tag{3}$$

$$\frac{p'(t)}{\rho c} = C_{nk} x(t) + D_n u'(t) \tag{4}$$

where

$$A_n = \begin{pmatrix} -\alpha_n & -\omega_n \\ \omega_n & -\alpha_n \end{pmatrix} \quad B_{nj} = \begin{pmatrix} 0 \\ \psi_n(x_j) \end{pmatrix}$$
$$C_{nk} = \begin{pmatrix} 0 & \frac{cA_j}{\Lambda_n}\psi_n(x_k) \end{pmatrix} \quad D_n = \begin{pmatrix} 0 \end{pmatrix}$$

The eigenvector of the duct for mode n is $\psi_n(k)$, the eigenvalue is ω_n, modal damping is α_n, speed of sound c, A_j is the input area and $\Lambda_n = \int \psi_n^2 dV$. It is straightforward to increase the number of modes. The pressure can be read out at an arbitrary position inside the duct by manipulating the matrix C_{nk}, and velocity inputs (p.e. from the loudspeaker) can be added by changing the matrix B_{nj}. Note that the transfer function from a velocity input to a pressure output at the same position will be minimum phase, whereas to a pressure output on the other side will be non-minimum phase. This is due to the time delay, which by a Padé approximation introduces non-minimum phase zeros.

3.2 *The Burner and the $L - \zeta$ Model*

ALSTOM's EV burner features flame stabilization in free space near the burner outlet due to sudden vortex breakdown of a swirling flow. The burner represents an obstacle to the flow, and an area change from A_1 to A_2 occurs at the dump plane. Linearizing the unsteady Bernoulli and the continuity equations and introducing an acoustic loss factor ζ and a reduced length L_{red} (accounting for capacitance effects) yields in matrix form

$$\begin{pmatrix} p'_2 \\ u'_2 \end{pmatrix} = T^b(s) \begin{pmatrix} p'_1 \\ u'_1 \end{pmatrix} \tag{5}$$

where $T^b(s)$ is a 2x2 matrix

$$T^b(s) = \begin{pmatrix} 1 & \rho c\left(M\left(1 - \zeta - \left(\frac{A_1}{A_2}\right)^2\right) - i\frac{\omega}{c}L_{red}\right) \\ 0 & \frac{A_1}{A_2} \end{pmatrix}$$

The subscripts 1 and 2 denote conditions up- and downstream of the element, respectively, M is the Mach number, c the speed of sound, and i the complex number.
It is hard to give a priori values for the loss factor ζ and the reduced length L_{red}, so they are found by a fit to experimental data (L_{red} is very close to the length of the burner). Note that two independent excitation experiments (up- and downstream) are necessary to determine all four elements of the matrix. Figure 2 shows the burner transfer function. The dynamic element is $T^b_{12}(s)$, relating the upstream velocity to the downstream pressure fluctuations.

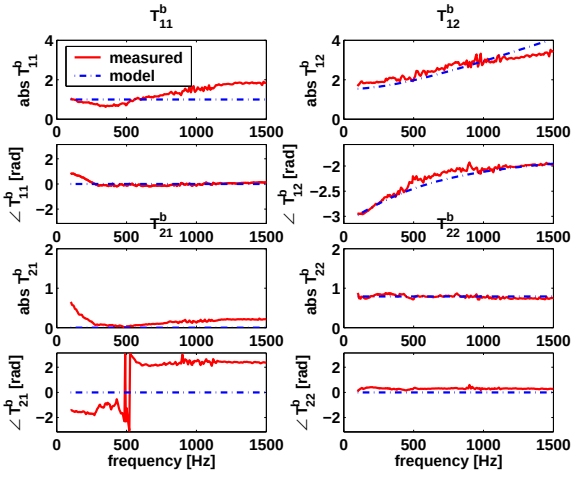

Fig. 2. The transfer function of the burner $T^b(s)$

3.3 *The Flame and the $n-\tau$ Model*

The flame is modelled as an acoustically compact element causing a jump in the acoustic velocity due to heat addition, whereas continuity of pressure is assumed. The key assumption is that velocity fluctuations at the burner cause heat release fluctuations, after a time delay τ (Schuermans *et al.*, 2004). In our premixed case, equivalence ratio fluctuations are not occurring, because the mixing happens so far upstream that pressure waves are unlikely to influence it. The $n-\tau$ model is given in matrix form

$$\begin{pmatrix} p_2' \\ u_2' \end{pmatrix} = \underbrace{\begin{pmatrix} 1 & 0 \\ 0 & 1+ne^{-i\omega\tau}e^{-\frac{1}{2}\omega^2\sigma_\tau^2} \end{pmatrix}}_{T^f(s)} \begin{pmatrix} p_1' \\ u_1 \end{pmatrix} \quad (6)$$

The time delay τ can be associated with a convective transport lag, but this value also admits a Gaussian distribution with a standard deviation σ_τ^2, which is represented by $e^{-\frac{1}{2}\omega^2\sigma_\tau^2}$. This value σ_τ^2 describes the geometrical shape of the flame (time-delay spread), and it is indeed observed that in order to be described accurately, longer flames require higher values of σ_τ^2. Figure 3 displays the measured transfer function of the flame. The dynamic element is $T_{22}^f(s)$, relating the upstream to the downstream velocity fluctuations.

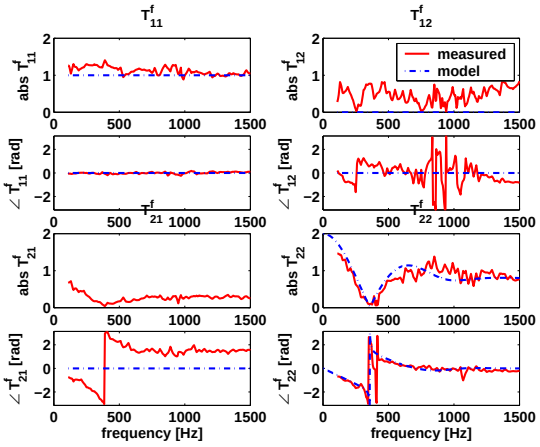

Fig. 3. The transfer function of the flame $T^f(s)$

3.4 *The Actuator and End Conditions*

For the present study, the actuator used is a loudspeaker introducing velocity perturbations. It is modelled as a high-pass filtered second-order system. A time delay of 0.42ms is added to this transfer function, which is related to the distance between the loudspeaker membrane and the middle of the duct.

The up- and downstream end conditions can be modelled as an acoustically closed and open boundary with admittance and impedance close to zero, respectively.

3.5 *Assembled Model*

The single blocks can now be assembled to yield the combustor transfer function, where the input is the voltage to the loudspeaker, and the outputs are the pressures read out at arbitrary positions in the ducts. As an example, the transfer functions $F_{ud}(s)$ and $F_{dd}(s)$ from the loudspeaker downstream at 0.303m to the microphone upstream at -0.072m and downstream at 0.213m are shown in figures 4 and 5, respectively. Low frequency non-minimum phase zeros are present in $F_{ud}(s)$, due to the bigger distance between actuator and sensor.

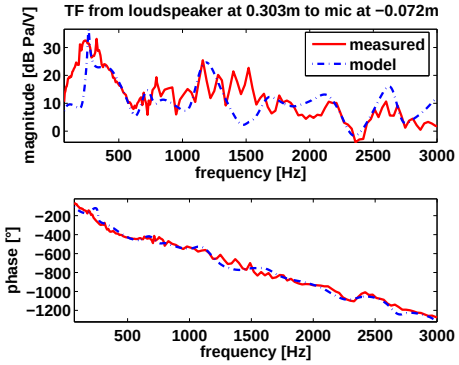

Fig. 4. The transfer function $F_{ud}(s)$ from the downstream loudspeaker to the microphone upstream of the burner

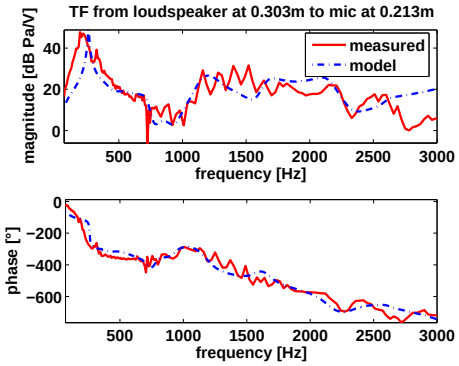

Fig. 5. The transfer function $F_{dd}(s)$ from the downstream loudspeaker to the downstream microphone

4. CONTROLLER DEVELOPMENT

4.1 *Fundamental Limits*

The non-minimum phase (NMP) zeros of $F_{ud}(s)$ have implications for the controller design process. As pointed out by many authors (see for instance (Skogestad and Postlethwaite, 1996)), a real NMP zero z limits the achievable bandwidth for feedback control to $\omega_c \lesssim z/2$. Good controller performance is again possible for $\omega_{c2} \gtrsim 2z$. On the other hand, right-hand-plane (RHP) poles require a minimum bandwidth $\omega_c \gtrsim 2p$ for real RHP

poles. It is clear that a real RHP pole p and a real NMP zero z have to satisfy $z \gtrsim 4p$ for acceptable controller performance. Time delays also pose fundamental problems. The "ideal" complementary sensitivity function for a time delay τ is $T = e^{-\tau s}$ (Skogestad and Postlethwaite, 1996), so the sensitivity function is $S = 1 - T = 1 - e^{-\tau s} \approx \tau s$ by a Taylor series expansion. S crosses the 0dB line for the first time at about $\omega = 1/\tau$, which determines the bandwidth. Another way of looking at it is to consider the first-order Padé approximation of a time delay $e^{-\tau s} \approx \frac{1-\tau/2s}{1+\tau/2s}$, which has a NMP zero at $2/\tau$, yielding again a bandwidth constraint of $\omega_c < \frac{z}{2} = \frac{2/\tau}{2} = 1/\tau$.

Another fundamental constraint to controller design is the so-called waterbed effect for systems with pole excess of at least two. The famous Bode integral states that

$\int_0^\infty ln|S(j\omega|d\omega = \pi \sum_{i=1}^{N_p} Re(p_i)$ where N_p is the number of RHP poles p_i and $Re(p_i)$ is the real part of them. It says that a sensitivity decrease over a frequency band always has to be compensated for with an equal (or even greater for unstable plants) increase in sensitivity at other frequencies. If actuator bandwidth constraints or model uncertainties exist, the sensitivity increase cannot be spread over an infinite frequency range, but sensitivity peaks necessarily occur.

If the system has NMP zeros, another "waterbed" formula is derived, which takes into account that the sensitivity increase and decrease have to happen over a limited frequency range $\omega < z/2$, yielding large peaks for $|S|$ if the sensitivity has to be decreased at low frequencies.

Another important constraint is actuator saturation. Whenever a plant cannot be stabilized in reality, even though in simulations, a linear controller can stabilize it, actuator saturation may be the culprit. Actuator bandwidth is often overlooked in controller design. As pointed out in (Freudenberg and Looze, 1985), a sensitivity decrease as well as an increase have to be completed within the actuator bandwidth. In other words, there must be a decrease in performance within a certain frequency band, due to feedback action.

4.2 H_∞-control

The H_∞-method is a powerful design tool allowing the control engineer to define bounds on the sensitivity and the complementary sensitivity by means of weighting functions added to the plant G_s and controller K to form an augmented plant. Figure 6 shows a setup known as $S/KS/T$ (Geering, 1999), where W_e weighs the sensitivity, W_u the control signal and W_y the complementary sensitivity. The control variables are represented by u, the measured variables by y, exogenous signals by w and error signals by z.

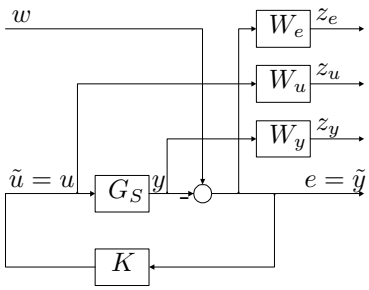

Fig. 6. A schematic diagram of the setup used to design an H_∞-controller

The H_∞-control synthesis procedure now consists of finding a controller K that stabilizes the closed-loop system and yields $\| T_{zw}(s) \|_\infty < \gamma = 1$. For the suggested $S/KS/T$ weighting scheme, the matrix T_{zw} is given by

$$T_{zw} = \begin{bmatrix} W_e S_e \\ W_u K S_e \\ W_y T_e \end{bmatrix} \tag{7}$$

which allows to weigh the sensitivity S_e with W_e, and the complementary sensitivity T_e by W_y. NMP zeros limit the achievable bandwidth, so that the transfer function $F_{dd}(ss)$ of the setup with downstream loudspeaker forcing and downstream pressure measurement is chosen. Moreover, a time delay of 0.42ms is limiting the bandwidth to about 400Hz.

Choosing the weights for the sensitivity W_e and the complementary sensitivity W_y as shown in Figure 7 (where the inverted weights are shown, which act as bounds if $\| T_{zw}(s) \|_\infty < \gamma = 1$), it can be verified that the achieved sensitivity and complementary sensitivity are indeed below the bounds, and the minimum value of S is about -14dB. The plot also shows the waterbed effect, where the sensitivity is simply shifted to other frequencies, but not destroyed. Hence a decrease in performance in the lower and higher frequency range is the price to pay in order to get the desired noise attenuation in the 160-370Hz band.

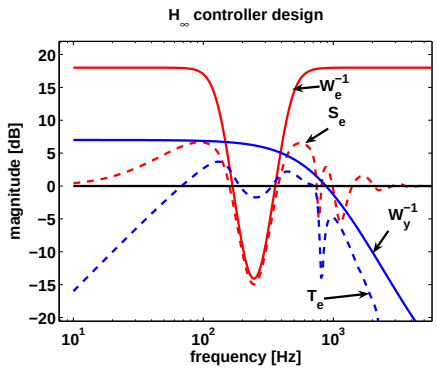

Fig. 7. The absolute value of the frequency response for S_e and T_e and the inverted weighting functions W_e^{-1} and W_y^{-1} acting as bounds

Figure 8 shows the frequency response of the resulting H_∞-controller. Control effort around 770Hz is demanded to accommodate the sensitivity increase.

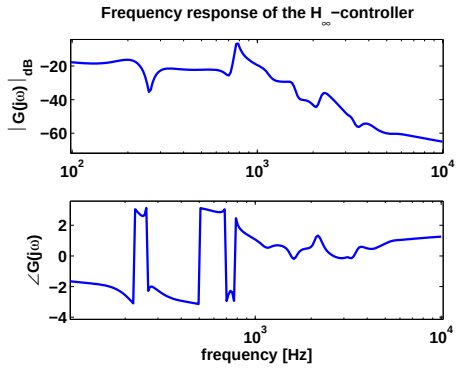

Fig. 8. The frequency response of the H_∞-controller

4.3 *Simulation Results*

The controller is state-reduced and tested in a Simulink simulation, resulting in the power spectral density plotted in Figure 9. The reduction in pressure achieved shows that the pressure could be reduced in the frequency range between 160Hz and 370Hz, at the expense of more noise at lower and higher frequencies. However, natural excitation is quite weak at these frequencies. It has also been verified that the control signal is not beyond the capabilities of the actuator.

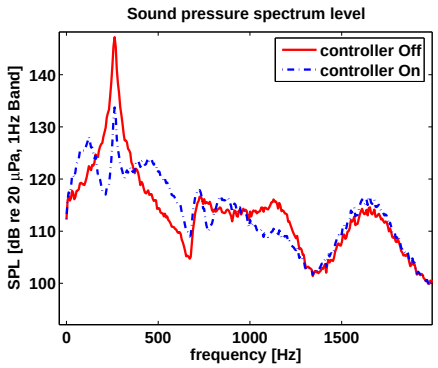

Fig. 9. The power spectral density with and without H_∞-controller

5. CONCLUSIONS

A model for the test rig at ETH has been derived based on physical modeling and experiments, which has been compared to measurements. It shows that relatively simple models are able to capture the dominant dynamics of the system. Fundamental limits hampering the controller development have been discussed. Finally, an H_∞-controller has been designed and tested in simulations, showing that good disturbance rejection is only possible in a limited frequency band due to time delays.

6. ACKNOWLEDGEMENTS

Financial support from ALSTOM Switzerland Ltd. is gratefully acknowledged. We would like to thank Daniel Fritsche and Marc Füri for their assistance with the test-rig.

7. REFERENCES

Annaswamy, A. M. and A. F. Ghoniem (2002). Active control of combustion instability: Theory and practice. *IEEE Control Systems Magazine* **22**(6), 37–54.

Campos-Delgado, D. U., K. Zhou, D. Allgood and S. Acharya (2003*a*). Active control of combustion instabilities using model-based controllers. *Combustion Science and Technology* **175**(1), 27–53.

Campos-Delgado, D.U., B.B.H. Schuermans, K.M. Zhou, C.O. Paschereit, E.A. Gallestey and A. Poncet (2003*b*). Thermoacoustic instabilities: Modeling and control. *IEEE Transactions on Control Systems Technology* **11**(4), 429–447.

Dowling, A. P. and S. R. Stow (2003). Acoustic analysis of gas turbine combustors. *Journal of Propulsion and Power* **19**(5), 751–764.

Freudenberg, J. S. and D. P. Looze (1985). Right Half Plane Poles and Zeros and Design Tradeoffs in Feedback-Systems. *IEEE Transactions on Automatic Control* **30**(6), 555–565.

Geering, H. P. (1999). *Robuste Regelung*. IMRT Press, Institut fuer Mess- und Regeltechnik, 8092 Zuerich.

Paschereit, C.O., E. Gutmark and W. Weisenstein (1999). Coherent structures in swirling flows and their role in acoustic combustion control. *Physics of Fluids* **11**(9), 2667–2678.

Rayleigh, Lord (1878). The explanation of certain acoustical phenomena. *Nature* **18**, 319:321.

Schuermans, B.B.H., V. Bellucci and C.O. Paschereit (2003). Thermoacoustic modeling and control of multi burner combustion systems. In: *ASME Turbo Expo*. Atlanta.

Schuermans, B.B.H., V. Bellucci, F. Guethe, F. Meili, P. Flohr and C.O. Paschereit (2004). A detailed analysis of thermoacoustic interaction mechanisms in a turbulent premixed flame. In: *ASME Turbo Expo*. Vienna, Austria.

Skogestad, S. and I. Postlethwaite (1996). *Multivariable Feedback Control: Analysis and Design Using Frequency-domain Methods*. John Wiley and Sons Ltd.